Publ. Astron. Soc. Japan 34, 199-221 (1982)

Neutral Hydrogen in M31. IV. Comparison with Optical Data and the Star Formation Rate

Naomasa NAKAI* and Yoshiaki SOFUE†

Department of Physics and Astrophysics, Nagoya University, Chikusa-ku, Nagoya 464

(Received 1981 September 8; revised 1981 December 14)

Abstract

Various optical features of population I objects in M31 are compared with the H I gas distribution obtained in Paper I. Most of H II regions, OB associations, and open clusters are distributed on ring-like H I main arms at galactocentric distances R=8–15 kpc which form a "10-kpc ring." The UV emission comes mostly from the 10-kpc ring. The outermost *trailing* H II spiral arm at R=18–26 kpc in the southwest is traced by OB associations and open clusters. The radial distributions of the young optical objects resemble that of the H I gas. However, a detailed comparison shows that younger objects are located in more inner regions than older objects. Dark nebulae are distributed mostly inside the 10-kpc ring.

A power law fitting of the densities of population I objects to the H I gas density in the form of

$$\rho(*)/10^{-9}\ \mathrm{pc}^{-3}=\kappa[\rho(\mathrm{H\ I})/1\ \mathrm{cm}^{-3}]^n$$

yields the coefficient values as $\log(\kappa)=1.86\pm0.07$, $n=2.06\pm0.10$ (R=0–20 kpc) for H II regions, $\log(\kappa)=1.19\pm0.11$, $n=1.93\pm0.11$ (R=0–30 kpc) for OB associations, $\log(\kappa)=1.43\pm0.08$, $n=1.84\pm0.08$ (R=0–30 kpc) for open clusters, where $\rho(*)$ and ρ(H I) are the number densities of the young objects and of H I atoms, respectively. Discussion is made of the star formation rate in M31. Propagation of a galactic-scale "star formation ring" is suggested.

Key words: Galaxies; M31; Neutral hydrogen; Population I tracers; Star formation.

1. Introduction

The spatial distribution of the H I gas in M31 as seen face-on has been obtained by Sofue and Kato (1981; hereafter referred to as Paper I) by applying the method of the velocity-to-space transformation (VST) to the data of high-sensitivity filled-aperture survey of the 21-cm H I line taken with the 100-m radio telescope by Cram et al. (1980) [see also Sawa and Sofue (1981; hereafter Paper II)]. The VST is a method with which the face-on distribution of the H I

* Present address: Department of Astronomy, University of Tokyo, Tokyo 113.
† Present address: Nobeyama Radio Observatory, Nobeyama, Minamisaku-gun, Nagano 384-13.

Table 1. Adopted parameters for M31.

Center position (1950)	R. A. $00^h\,40^m\,00^s$
	Decl. 41° 00′ 00″
Position angle of the major axis	38°
Inclination (90° is edge-on)	77°
Distance	690 kpc
Systemic radial velocity	-300 km s^{-1}

gas in a largely tilted (nearly edge-on) disk galaxy is determined from radial velocity data. The resulting H I map is reproduced in figures 1–6 from Paper I. Some parameters of M31 are given in table 1.

In the present paper we compare the H I distribution with optical features of M31 to examine correlation between them. We also aim at obtaining the rate of star formation in M31. Compared with earlier studies of correlation between optical and H I data (Emerson 1974; Berkhuijsen 1977; Unwin 1980a, b), our study has several characteristics: (a) As the observation of the H I gas was made with a filled-aperture telescope, sensitivity is high even for the diffuse component of the gas, and the spatial limit of detection reaches about 30 kpc from the center of M31. (b) As the VST method has been used, the spatial resolution along the minor axis has been improved by a factor of four compared with the antenna half-power width. (c) Several kinds of new and large amount of data, namely those of H II regions, OB associations, open clusters, dark clouds, a UV photograph, and supernova remnants as well as X-ray sources, are used.

2. Comparison between Optical Data and H I Gas Density

We compare the distribution of the H I gas obtained in Paper I with various optical features of M31. The spatial resolution of the H I map in figures 1–6 is approximately $\Delta\xi\times\Delta\eta=1.8\times1.5$ kpc, except near the minor axis at $|\xi|<3$ kpc, where $\Delta\eta>3$ kpc. An uncertainty of the H I distribution occurs near the ξ-axis at $|\eta|<4$ kpc (see Paper I). Here ξ and η are the distances on the galaxy plane parallel and perpendicular to the major axis, respectively. Face-on distributions of optical objects are obtained by simple de-projection onto the plane of the galaxy by assuming the parameters in table 1.

i) Visible and UV Images

Figure 1 (reproduced from Paper I) shows a contour map of the surface column density of the H I gas superposed on the Palomar Sky Survey print (blue). The contour map is a projection onto the plane of the sky with an inclination angle of 77° (Paper I). The figure shows that the H I gas extends to a distance as large as 30 kpc from the center, almost twice as broad as the optical image. The main H I arms at radii $R=8$–15 kpc are accompanied by optical arms. However, there is no obvious optical counterpart to the outermost spiral arm of the H I gas in SW (southwest) at $R=18$–26 kpc.

Recently Deharveng et al. (1980 and private communication) obtained a UV image of M31 from a balloon-borne experiment. Figure 2 shows the UV photograph with a map of the H I gas superimposed. The UV image except for the central region shows a ring-like structure at $R\simeq10$ kpc and coincides with the main H I ring (the 10-kpc ring) except in the western part. The correlation between the outer H I gas and a weak outer ($R\simeq16$ kpc) arm of UV, which ex-

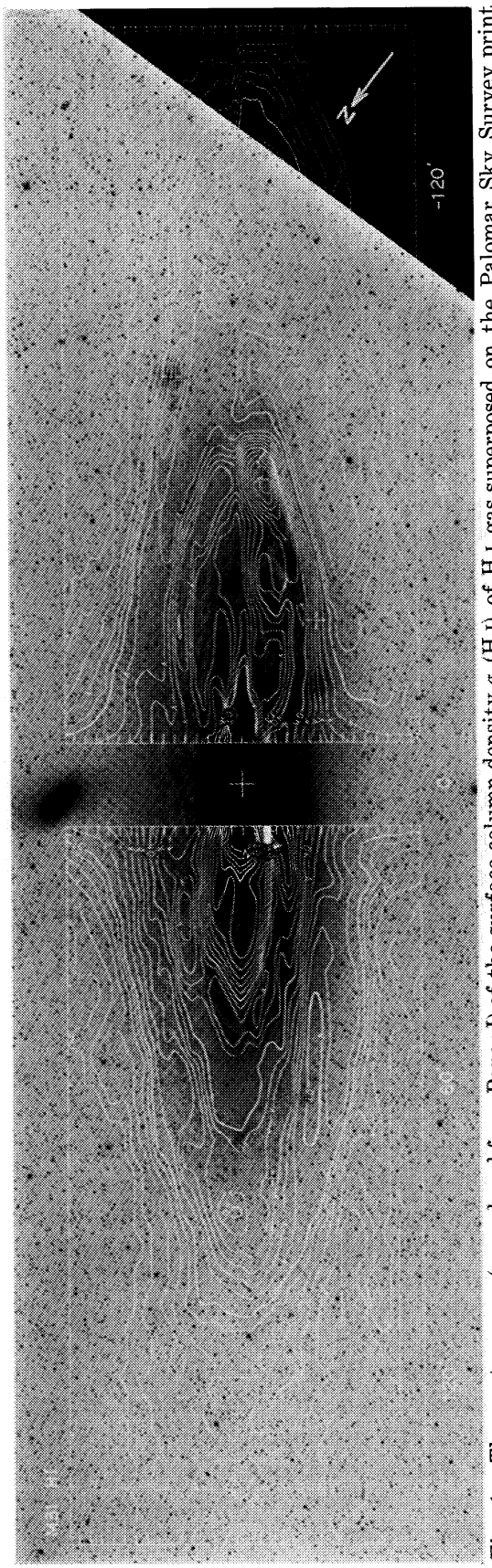

Fig. 1. The contour map (reproduced from Paper I) of the surface column density σ_N(H I) of H I gas superposed on the Palomar Sky Survey print (blue). The contour map is a projection onto the plane of the sky with an inclination angle of 77°. The contour units are in 10^{19} atoms cm^{-2}.

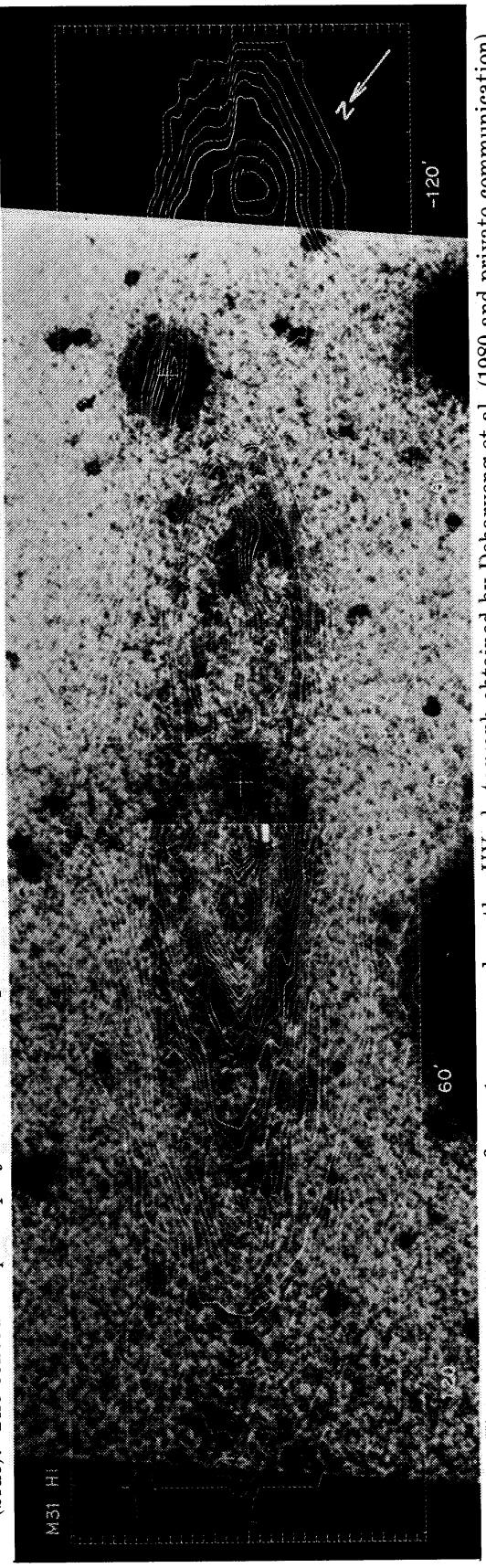

Fig. 2. The same contour map as figure 1 superposed on the UV photograph obtained by Deharveng et al. (1980 and private communication).

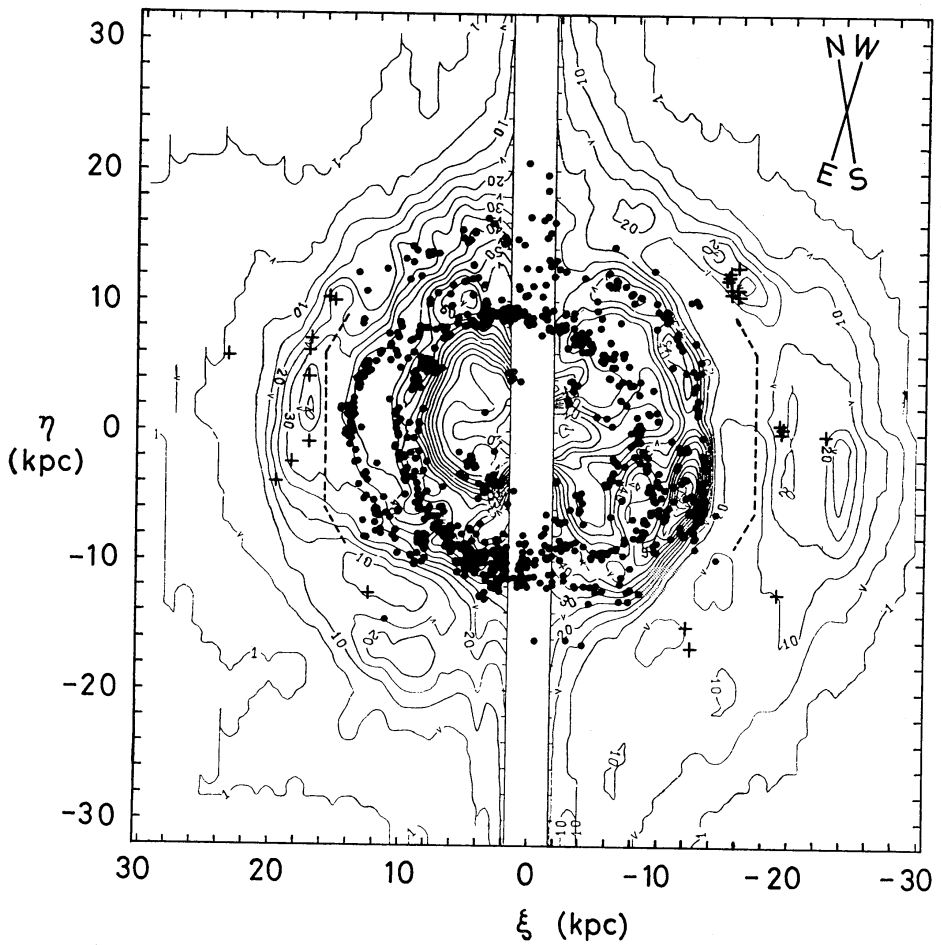

Fig. 3. The face-on contour map of σ_N(H I) superposed on the positions of H II regions cataloged by Pellet et al. (1978) ($-79' < \xi < 86'$), marked with circles, and by Baade and Arp (1964) ($\xi < -79'$, $86' < \xi$), marked with crosses. Two dashed lines indicate $\xi = -79'$ and $86'$.

tends from NW (northwest) toward N (north) is not clear, although there are several spur-like features of the H I gas.

ii) H II Regions

Figure 3 shows a contour map of the surface column density of the H I gas superposed on the positions of 981 H II regions obtained by Pellet et al. (1978) [see also Simien et al. (1978)]. Two dashed lines in the figure indicate the limits of their Hα photographs ($-79' < \xi < 86'$). H II regions generally lie along the main H I arms at R=8–15 kpc. H II regions with high-surface brightness [Pellet et al. (1978); see also figure 7] are concentrated on the strong condensations of the H I gas with $\sigma_N(\text{H I}) > 6 \times 10^{20}$ cm^{-2} at $(\xi, \eta) \simeq$(5 kpc, 11 kpc), (3 kpc, -7 kpc), and (-12 kpc, -5 kpc) in the H I ring. Few H II regions lie in the inner region ($R <$ 8 kpc) where H I emission is weak. On scales of less than 2 kpc, strings of H II regions appear to avoid the brightest peaks of H I emission, but it is not clear whether this tendency is significant from our spatial resolution of the H I map.

On the SW ($R \simeq$18–26 kpc), NE ($R \simeq$17 kpc), and eastern outer ($R \simeq$20 kpc) arms, H II regions are not cataloged by Pellet et al. (1978). Baade and Arp (1964) and Arp (1964) have cataloged several H II regions in these outer regions

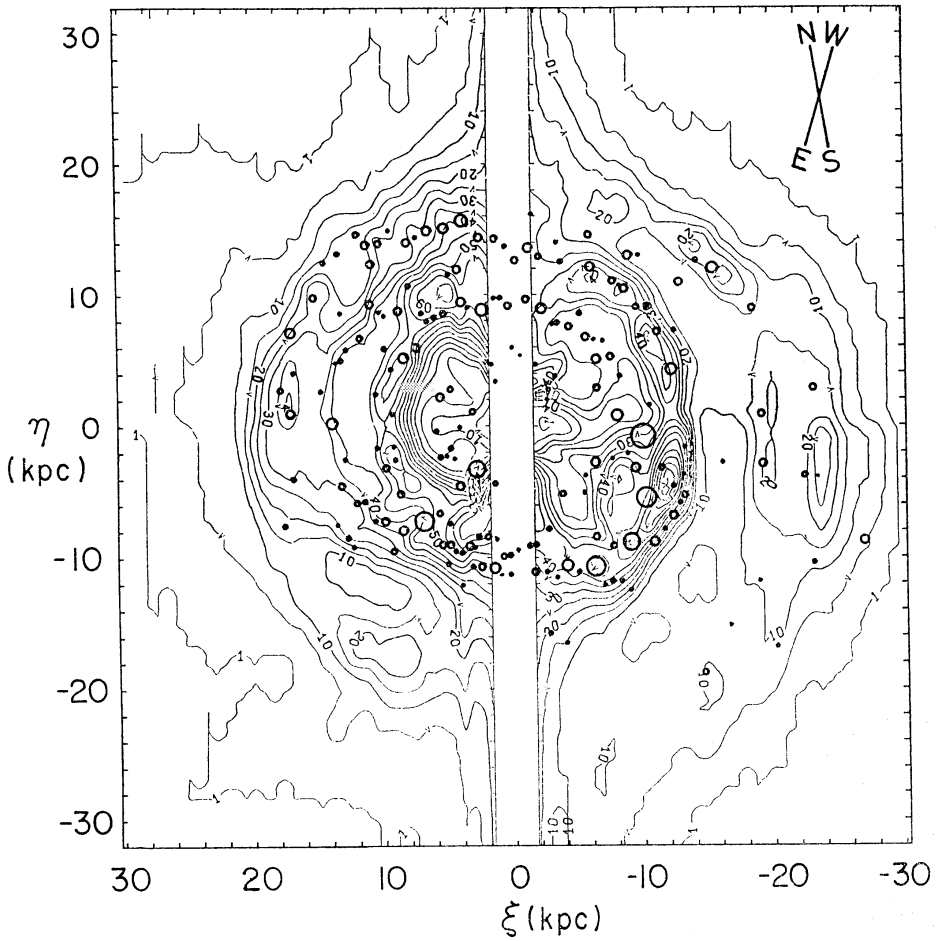

Fig. 4. The contour map of σ_N(H I) superposed on the distribution of OB associations listed by van den Bergh (1964) and Richter (1971). The sizes of the circles indicate approximate dimensions of OB associations.

located on the H I outer arms.

iii) OB Associations

Figure 4 shows a contour map of the surface column density of the H I gas superposed on the distribution of 195 OB associations listed by van den Bergh (1964) and Richter (1971). There is also agreement between the large-scale distributions of the H I gas and OB associations in the main arms. Van den Bergh (1964) classified OB associations according to their clumpiness into "young," "intermediate," and "old." Many of "young" OB associations lie along the main H I arms, especially near the three strong H I condensations [σ_N(H I)$>6\times10^{20}$ cm^{-2}] in the arms mentioned above. It is worthwhile to note that the SW (R=18–26 kpc) and NE outer ($R\simeq$17 kpc) arms are generally traced by several OB associations. No OB association exists in the region of σ_N(H I)$<5\times10^{19}$ cm^{-2}.

iv) Open Clusters

Figure 5 shows the H I distribution together with the positions of about 400 open star clusters cataloged by Hodge (1979 and private communication). Many of open clusters also lie on the main H I arms. However, the distribution of open clusters is wider and reaches the regions of lower surface H I density

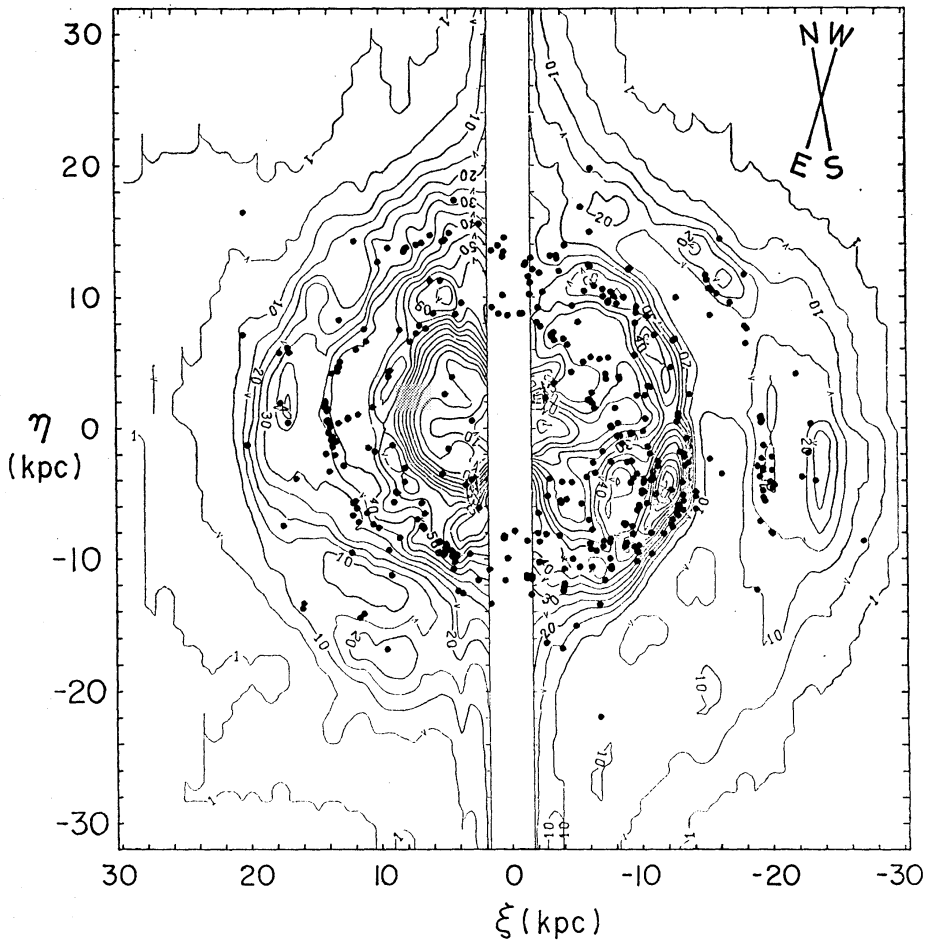

Fig. 5. The contour map of σ_N(H I) superposed on the positions of open star clusters cataloged by Hodge (1979 and private communication).

[σ_N(H I)$>2\times10^{19}$ cm^{-2}] compared with H II regions and OB associations (also see section 3). Moreover a large number of open clusters trace clearly the SW outer arm and are crowded around the regions of high surface H I density [σ_N(H I)$>2\times10^{20}$ cm^{-2}] at $(\xi, \eta)=(-20$ kpc, -3 kpc) and (-16 kpc, 11 kpc). This fact means that star formation occurs even in the SW outer arm.

v) Supernova Remnants

D'Odorico et al. (1980) have cataloged 19 candidates of supernova remnant in M31. They note that most of the candidates are identified with compact H II regions cataloged by Pellet et al. (1978). In figure 6 we superpose the positions of the SNR candidates on the H I map. The figure shows that most of the SNR are located on the H I arms and coincide with the principal features traced by H II regions, OB associations, and open clusters (see also figure 7).

vi) X-Ray Sources

Recent X-ray observations of M31 with the Einstein Observatory (Van Speybroeck et al. 1979) have shown that there are 21 sources in a compact inner bulge of the galaxy, 40 sources which are categorized as population I, seven globular clusters, and 8 sources near globular clusters. Unfortunately the observed fields cover a limited portion of the M31 disk so that their data are not enough

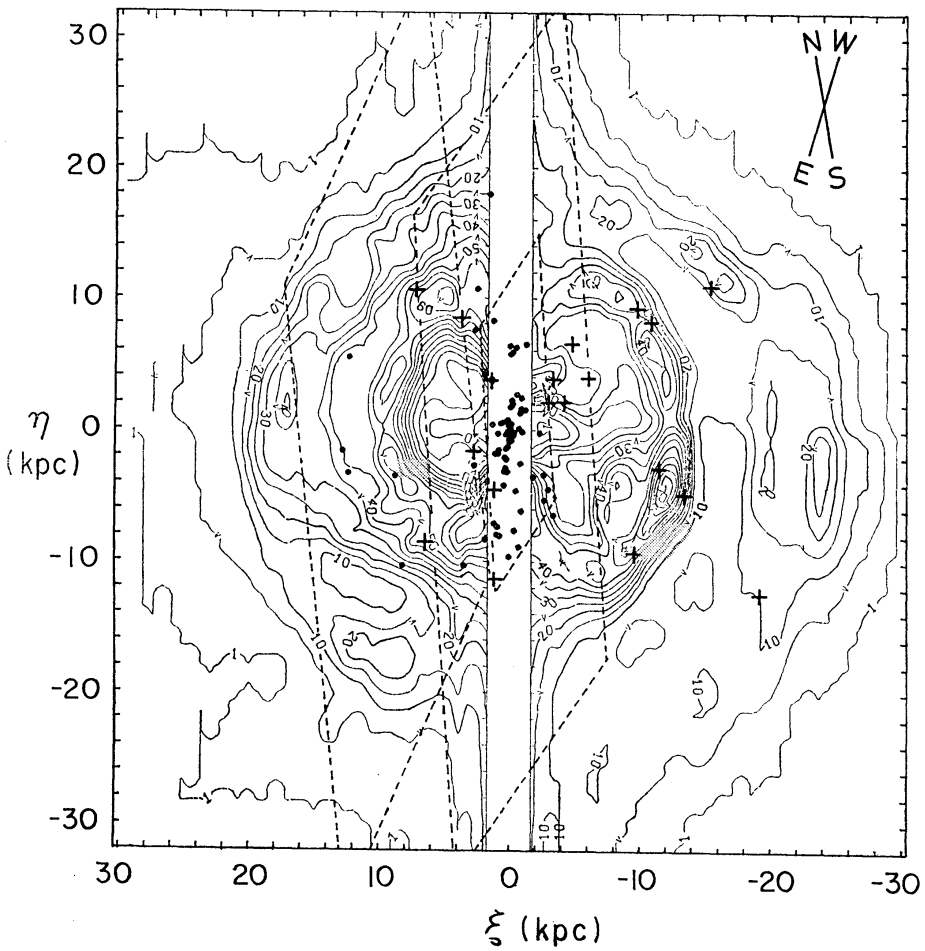

Fig. 6. The contour map of σ_N(H I) superposed on the positions of the candidates of supernova remnant (crosses) identified by D'Odorico et al. (1980) and X-ray sources (dots) cataloged by Van Speybroeck et al. (1979). Three observed fields for X-ray sources are indicated by the dashed lines. The X-ray sources include 21 sources in a compact inner bulge, 40 population I sources, seven globular clusters and eight sources near the globular clusters.

for the present correlation analysis among various features of M31. However, Van Speybroeck et al. (1979) claim that the population I X-ray sources are associated with bright visible objects, neutral hydrogen, dusts, and other population I tracers. Figure 6 shows superposition of the X-ray sources on the H I map. Except for the sources associated with globular clusters and the inner bulge component, the sources, which are mostly population I, trace well the principal features of the H I gas.

vii) The Relations among the Optical Features

Figure 7 shows the superposition of the outlines of the H II regions, OB associations, dark clouds with maximum dimensions $D>1.^{\circ}5$(300 pc) (Hodge 1980), the candidates of supernova remnant, and X-ray sources. Remarkable relations among these objects are as follows. (a) Most of OB associations are accompanied by H II regions. OB associations and H II regions make up the same arms. (b) Many H II regions with high surface brightness ($S>1.0\times10^{-5}$ erg cm^{-2} s^{-1} sr^{-1}) cluster around the regions of $(\xi, \eta)=$(5 kpc, 11 kpc), (3 kpc, -7 kpc), and (-12 kpc,

-5 kpc) where young OB associations also cluster and the surface column density of the H I gas is highest [$\sigma_N(\mathrm{H\,I})>6\times10^{20}\,\mathrm{cm}^{-2}$]. (c) Dark clouds generally lie on the inner edges of strings of H II regions and OB associations. (d) Both H II regions and OB associations form an arm at $R\simeq5$ kpc except in the southern quadrant. The dark clouds trace most of this "5 kpc arm." (e) In the southern part at $R\simeq12$ kpc, H II regions and dark clouds lie on the inner edges of the string of OB associations of the intermediate age class [OB 82 to OB 86 in van den Bergh's (1964) catalog]. (f) Supernova remnants lie on the spiral arms. (g) Population I X-ray sources also lie on the spiral arms. An X-ray source at $(\xi, \eta)=$ (1.6 kpc, 3.8 kpc) coincides with a supernova remnant.

3. Radial Distributions

In this section we obtain radial distributions of the H II regions, OB associations, open clusters, and dark clouds, and compare them one another with that of the H I gas.

i) H II Regions

Pellet et al. (1978) cataloged 981 H II regions with their coordinates, dimensions, surface brightness divided into three classes, and other information. Using the data, we can obtain the surface number density, the area ratio, the surface mass density, and the surface photon density of H II regions on the plane of M31 averaged in each of the circular rings of 1-kpc width concentric with the galactic center as a function of distance R. Here, the area ratio means the ratio of the area occupied by H II regions to the area of each of the rings. The mass of an H II region and the number of Lyman photons radiated by the central stars in an H II region are obtained as follows: The emission measure EM is obtained from the surface brightness S, taking the electron temperature as 10^4K (Pellet et al. 1978). EM gives the number density of electrons n_e, if we assume the thickness of an H II region. It is assumed that an H II region is composed of the perfectly ionized hydrogen gas, so that the ion number density n_H is equal to n_e. Then the mass of an H II region and the Lyman photon number emitted by stars in the H II region can be obtained from n_e, n_H, and the size of the H II region (Spitzer 1978). Here we assume that the H II region has an ellipsoidal shape.

Figures 8a and 8b show the radial distributions of the surface number density and the area ratio, respectively. Figures 8a and 8b show a peak around $R\simeq10$ kpc. However, the concentration around 10 kpc in figure 8b is higher than in figure 8a. This is because larger H II regions are more concentrated at $R=8$–11 kpc (see figure 3). The distribution of the surface mass density of H II regions is presented in figure 8c. The concentration at $R=8$–11 kpc is more remarkable. There are two largest H II regions, No. 184 and No. 621 [notation by Pellet et al. (1978)]: The mass of No. 184 at $R=8.0$ kpc is $4.6\times10^6M_\odot$ which is about two thirds of the total mass of H II regions in the $R=8$–9 kpc ring. The mass of No. 621 at $R=10.7$ kpc is $2.7\times10^6M_\odot$ and is about a third part of the total mass of H II regions in the $R=10$–11 kpc ring. Figure 8d shows the surface photon number density emitted from stars in the H II regions. The amount of the Lyman photon emission at $R=8$–12 kpc is about 70% of the total Lyman photons due to H II regions in M31.

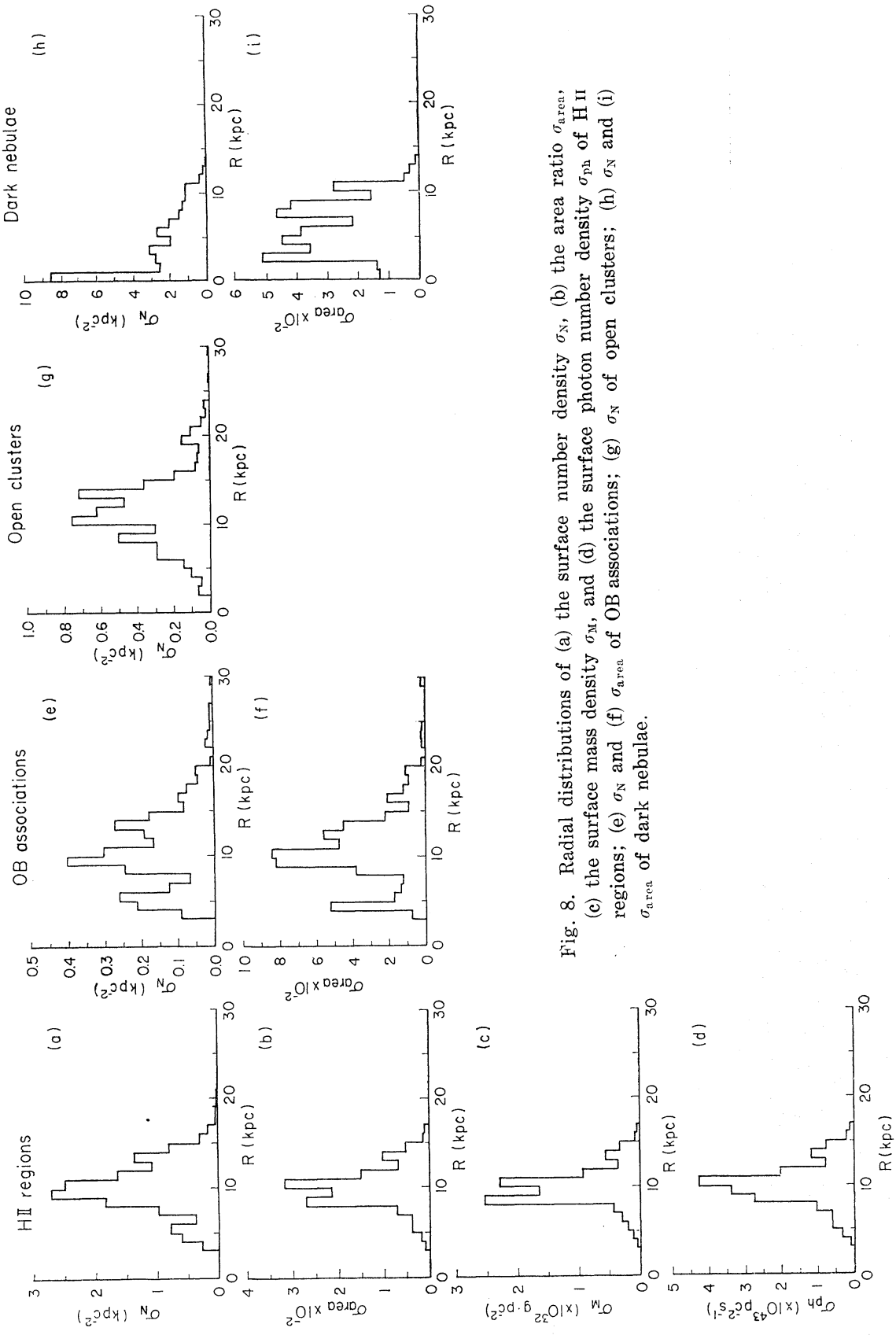

Fig. 8. Radial distributions of (a) the surface number density σ_N, (b) the area ratio σ_{area}, (c) the surface mass density σ_M, and (d) the surface photon number density σ_{ph} of H II regions; (e) σ_N and (f) σ_{area} of OB associations; (g) σ_N of open clusters; (h) σ_N and (i) σ_{area} of dark nebulae.

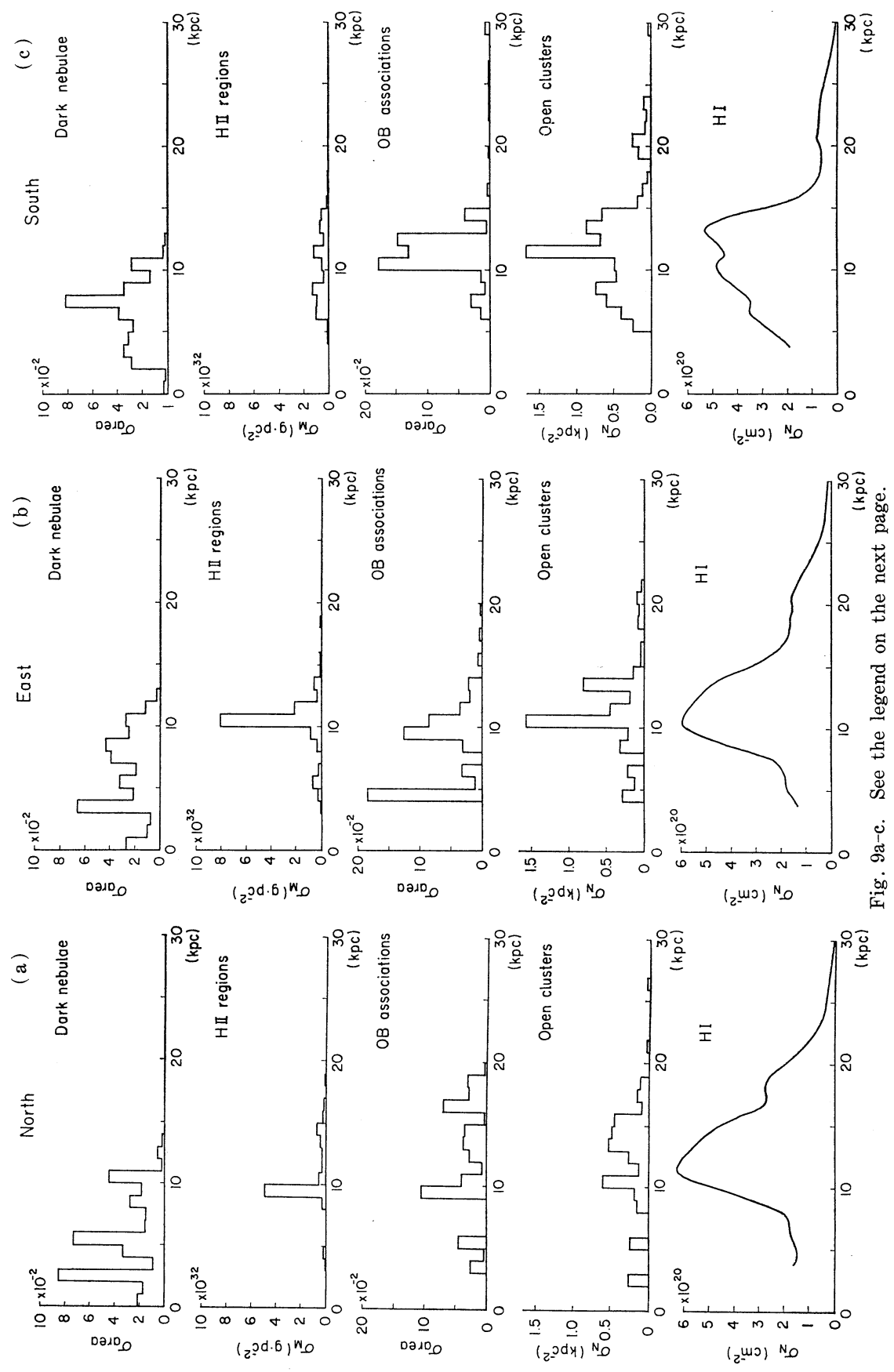

Fig. 9a–c. See the legend on the next page.

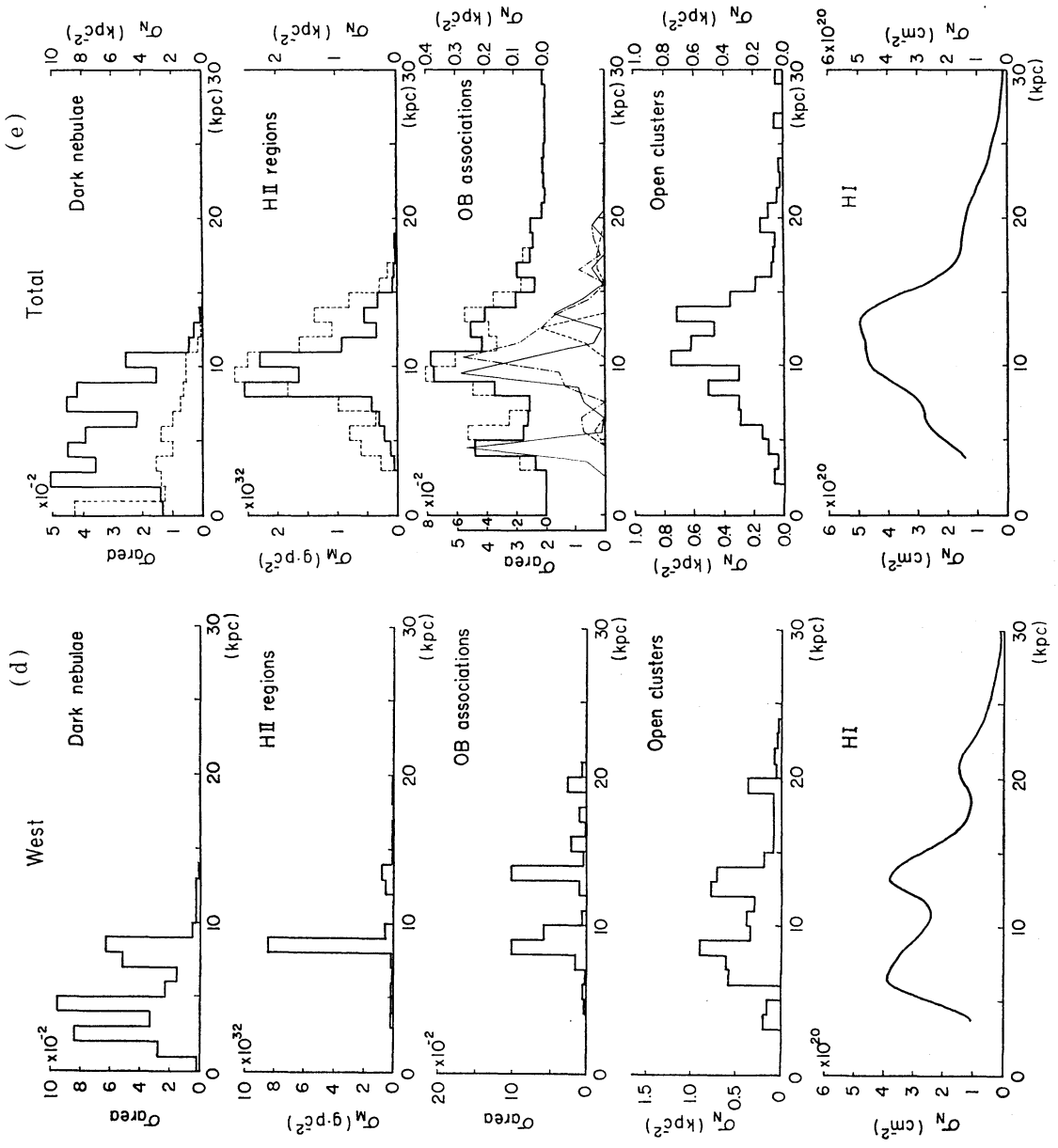

Fig. 9. Radial distributions of dark nebulae, H II regions, OB associations, open clusters, and H I gas averaged over each of the four sectors divided by the ξ and η axes: (a) northern; (b) eastern; (c) southern; and (d) western quadrants; and (e) those averaged all round the galaxy. In figure (e) dashed lines of dark nebulae, H II regions, and OB associations represent distributions of σ_N. Distributions of young, intermediate age, and old OB associations are also shown separately with the full line, dash-dotted line, and dashed line, respectively.

ii) OB Associations

Figures 8e and 8f show the radial distributions of the surface number density and the area ratio of 195 OB associations listed by van den Bergh (1964) and Richter (1971). The distributions have two main peaks at 5 kpc and 10 kpc and decreases outward. The peaks at 5 kpc and 10 kpc correspond to the "5-kpc arm" as discussed in the previous section and to the "10-kpc ring," respectively. Some OB associations are located in very outer regions as far as 30 kpc from the center.

iii) Open Clusters

As to open clusters we know only the positions [Hodge (1979 and private communication)]. The radial distribution of the surface number density is shown in figure 8g. Open clusters have the tendency to distribute in more outer regions than H II regions and OB associations [see subsection v(5)], and the degree of concentration over intermediate distance ($R\sim10$ kpc) is weaker. A peak at $R\simeq20$ kpc corresponds to the SW outer arm.

iv) Dark Clouds

Figures 8h and 8i show the radial distributions of the surface number density and the area ratio of 730 dark clouds identified by Hodge (1980). Figure 8h gives an impression as if dusts were concentrated in the center of the galaxy. However, the distribution in figure 8i varies dramatically compared with that in figure 8h, and has some peaks corresponding to dark lanes in visual-light photographs. We note that the dark-cloud distribution in figure 8i has two peaks at $R\simeq4$ kpc and $R\simeq8$ kpc which are respectively located on the inner sides of the "5-kpc arm" and the "10-kpc ring."

It must be kept in mind that the detection of a dark cloud depends on the background and foreground star-lights. There is a possibility of missing dark clouds at the outer part where the background light is weak. Hodge (1980) points out that the number of dark clouds on the far (south) side of the galaxy is three quarters of that on the near (north) side, and many dark clouds are obscured by the intervening bright star-lights in the halo. A dark cloud whose size is smaller than the resolution of observation ($\simeq5''=17$ pc) also cannot be detected.

v) Comparison among Radial Distributions

In figure 9 we compare the radial distribution of the surface H I gas density with those of the surface densities of dark clouds and young objects. They are compared separately for (a) northern, (b) eastern, (c) southern, and (d) western quadrants of M31 disk as well as (e) all around the galaxy. We may note some remarkable relations among the distributions:

(1) The radial distributions of H II regions, OB associations, open clusters, and the H I gas generally agree with each other.

(2) In the northern quadrant, however, optical objects at $R=10$–15 kpc seem to be distributed on either side of the peak of the H I gas (figure 9a).

(3) In most of the arms the older OB associations are distributed farther away from the galactic center than younger ones (figure 9e).

(4) The weighted mean radii $\bar{R}$ of the radial distributions increase in the order of H II regions, OB associations, open clusters, and the H I gas (see figure 9e and table 2). Namely $\bar{R}$ (H II regions)$=10.1$ kpc, $\bar{R}$ (OB associations)$=10.7$ kpc,

and $\bar{R}$ (open clusters)=11.5 kpc.

(5) The concentration of H II regions around the weighted mean radius $\bar{R}$ is higher than those of OB associations and open clusters (figure 9e and table 3).

(6) A general correlation between the radial distributions of dark clouds and other optical objects can be recognized at $R=5$–12 kpc. Few dark clouds are detected at $R>12$ kpc. In the inner region at $R<5$ kpc only a few optical objects corresponding to dark clouds are found. The correlation of dark clouds with the H I gas at $R<5$ kpc is ambiguous because of low H I density and poor spatial resolution of the H I map in the inner region of M31.

Table 2. The weighted mean radii $\bar{R}$ of the radial distributions.

Object	$\bar{R}$ (kpc)			
	σ_N	σ_{area}	σ_M	σ_{ph}
H II regions	10.1	10.1	9.9	10.1
OB associations	10.7	10.9	—	—
Open clusters	11.5	—	—	—
H I gas	12.5	—	—	—

The tendencies of optical objects in relations (4) and (5) seem to be related to the difference in the ages τ of the objects: $\tau \simeq 10^5$–10^7 yr for H II regions, $(1.5\text{–}4)\times 10^7$ yr for OB associations, and 10^6–10^8 yr for open clusters. Hodge (1979) has also examined the radial distribution of the ratio of the numbers of "old" (10^8 yr) to "young" (10^6 yr) clusters along the major axis and pointed out the tendency for the older clusters to be relatively more plentiful at greater distances (say $R>15$ kpc). These facts, in particular relations (3) and (4), suggest a large-scale (galactic scale) shifting, or propagation, of the star formation sites toward the galactic center: about 10^7–10^8 yr ago the star formation was most active in more outer regions centered at $R\simeq 11$–12 kpc, while the current star formation has been enhanced mostly around the "10-kpc ring" at $R\simeq 10$ kpc. If this picture is correct, the speed of the propagation of star formation sites (the "star formation ring") is approximately 1–2 kpc per 10^7–10^8 yr, namely at 10–100 km s^{-1}.

4. The Rate of Star Formation

A quantitative examination of the correlation between the distributions of the H I gas and optical young objects can be used to obtain the rate of star formation from the gaseous matter in a galaxy (e.g. Smith et al. 1978; Talbot 1980). Several authors have attempted to obtain the formation rate in M31 by comparing optical data of H II regions with H I gas data mainly taken with interferometers (Emerson 1974; Guibert 1979; Unwin 1980a, b). However, interfer-

Table 3. Degree of concentration around the weighted mean radius $\bar{R}$ and typical ages of the young objects.

Object		Degree of concentration* (%)				Age (yr)
		σ_N	σ_{area}	σ_M	σ_{ph}	
H II regions	(R=8-12 kpc)	56	69	76	69	10^5-10^7
OB associations	(R=9-13 kpc)	36	50	—	—	$(1.5\text{-}4)\times 10^7$
Open clusters	(R=10-14 kpc)	47	—	—	—	10^6-10^8
H I gas	(R=10-14 kpc)	39	—	—	—	

* Fraction of the sum of surface densities in a ring of 4-kpc wide centered on $\bar{R}$ against the sum in the whole galactic plane.

ometric observations lack information about the gas distribution of scales greater than the lowest spatial resolution determined by the shortest spacing of antennas. This implies that the H I gas densities inferred from interferometric observations do not show "absolute" values, or always give underestimated values. On the other hand, observations using filled-aperture radio telescopes, which are the case for our H I map in figures 1–6, are equally sensitive to any scale distribution larger than the spatial resolution. In particular, our H I map is valid even for such a large-scale distribution extending to $R \simeq 30$ kpc. Therefore the H I densities derived from filled-aperture observations are more reliable to derive quantities such as the star formation rate.

We here derive the rate of star formation by comparing the H I map not only with the H II regions but also with OB associations and open clusters. The rate of star formation is assumed to follow a power law against the gas density (Schmidt 1959):

$$d\rho_{\rm M}(*)/dt = \kappa \rho_{\rm M}{}^{n}({\rm gas}) \ , \tag{1}$$

where $\rho_{\rm M}(*)$ is the total mass of stars in unit volume, $\rho_{\rm M}({\rm gas})$ is the density of the gas, and κ and n are constants. We may obtain a typical star formation rate through the mass of stars involved in an H II region divided by its typical age, τ(H II). Namely we can calculate $d\rho_{\rm M}(*)/dt$ through

$$d\rho_{\rm M}(*)/dt \simeq \rho_{*{\rm M}}({\rm H\ II})/\tau({\rm H\ II}) \ , \tag{2}$$

where $\rho_{*{\rm M}}$(H II) is the mean density of stars involved in H II regions. In general it is difficult to estimate the mass of stars involved in an H II region, OB association, or open cluster. Therefore we replace $\rho_{*{\rm M}}$(H II) by the number density $\rho_{\rm N}$(H II) of H II regions, assuming that masses of stars in all H II regions are same, namely,

$$\rho_{*{\rm M}}({\rm H\ II}) \simeq \rho_{\rm N}({\rm H\ II}) m({\rm H\ II}) \ , \tag{3}$$

where m(H II) is a typical mass of stars in the H II region. Therefore, we have from equations (2) and (3)

$$d\rho_{\rm M}(*)/dt \simeq \rho_{\rm N}({\rm H\ II}) m({\rm H\ II})/\tau({\rm H\ II}) \ . \tag{4}$$

Similar relations can be written for the area ratio $\rho_{\rm area}$(H II), the mass density of H II regions $\rho_{\rm M}$(H II), or number density of emitted photons $\rho_{\rm ph}$(H II) from stars in H II regions, supposing that the mass of stars in an H II region is proportional to the area or the mass of the H II region, or to the photon number radiated from the H II region.

If the thickness of the galactic disk in which the star formation takes place is constant, we may replace the volume densities by the surface density, $\sigma_{\rm M}(*)$, of young stars and that of H II regions, $\sigma_{\rm N}$(H II):

$$d\sigma_{\rm M}(*)/dt = \sigma_{\rm N}({\rm H\ II}) m({\rm H\ II})/\tau({\rm H\ II}) \ . \tag{5}$$

Equation (5) can be related to the observed H I surface density, $\sigma_{\rm N}$(H I), through equation (1):

$$\sigma_{\rm N}({\rm H\ II}) m({\rm H\ II})/\tau({\rm H\ II}) = \kappa \sigma_{\rm N}({\rm H\ I})^{n} \ , \tag{6}$$

where both $\sigma_{\rm N}$(H II) and $\sigma_{\rm N}$(H I) are known from observations directly. Similar re-

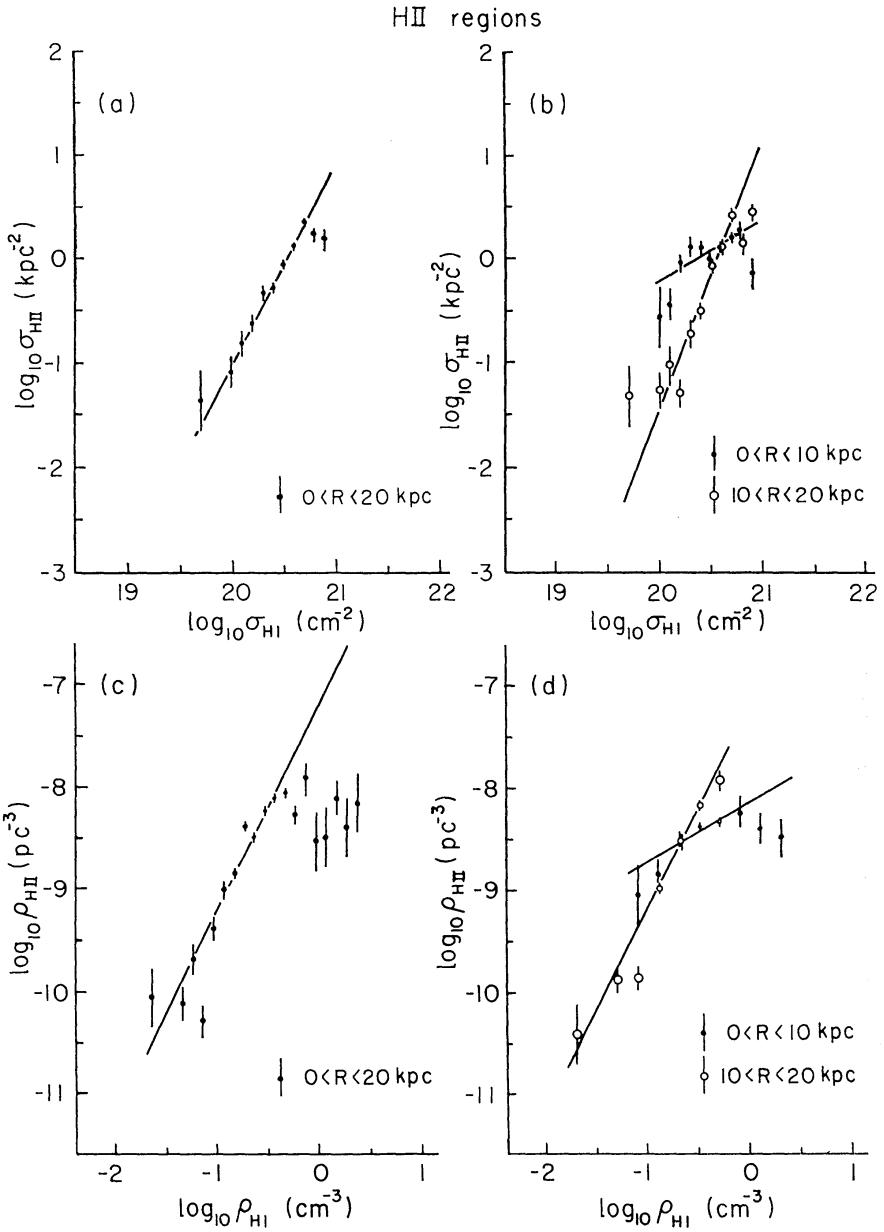

Fig. 10. The relation between σ_N(H II) and σ_N(H I) for (a) the whole galaxy and for (b) $0<R<10$ kpc and $10<R<20$ kpc, and the relation between ρ_N(H II) for ρ_N(H I) for (c) the whole galaxy and (d) $0<R<10$ kpc and $10<R<20$ kpc. The straight line shows the least-squares fit by a power-law relation.

lations are obtained for OB associations and open clusters, respectively, as

$$\sigma_N(\mathrm{OB})m(\mathrm{OB})/\tau(\mathrm{OB})=\kappa\sigma_N(\mathrm{H\,I})^n\,, \tag{7}$$

and

$$\sigma_N(\mathrm{oc})m(\mathrm{oc})/\tau(\mathrm{oc})=\kappa\sigma_N(\mathrm{H\,I})^n\,. \tag{8}$$

4.1. The Rate of Star Formation Derived from the Surface Densities

i) H II regions

To calculate the surface number density σ_N(H II) of H II regions, we divide

Table 4. Relation between surface densities of H II regions and H I gas defined by $[\sigma(\mathrm{H\,II})/\sigma^0(\mathrm{H\,II})]=\kappa[\sigma_N(\mathrm{H\,I})/\sigma_N{}^0(\mathrm{H\,I})]^n$, where $\sigma(\mathrm{H\,II})$ represents $\sigma_N(\mathrm{H\,II})$, $\sigma_{area}(\mathrm{H\,II})$, $\sigma_M(\mathrm{H\,II})$, or $\sigma_{ph}(\mathrm{H\,II})$ (see the text), and $\sigma_N{}^0(\mathrm{H\,I})$ is taken as $10^{20}\,\mathrm{cm}^{-2}$.

Physical quantity $[\sigma^0(\mathrm{H\,II})]$	Class[1]	Radius range (kpc)	log κ	n
$\sigma_N(\mathrm{H\,II})$ $(\sigma_N{}^0=1.0\,\mathrm{kpc}^{-2})$	All	0-20	-1.02 ± 0.06	1.94 ± 0.11
	All	0-10	-0.20 ± 0.07	0.60 ± 0.13
	All	10-20	-1.42 ± 0.09	2.61 ± 0.15
	Class 1	0-20	-1.27 ± 0.07	1.88 ± 0.13
	Class 2	0-20	-1.54 ± 0.08	1.90 ± 0.14
	Class 3	0-20	-1.89 ± 0.13	2.32 ± 0.26
$\sigma_{area}(\mathrm{H\,II})$ $(\sigma_{area}{}^0=0.01)$.....	All	0-20	-1.25 ± 0.09	2.38 ± 0.18
$\sigma_M(\mathrm{H\,II})$ $(\sigma_M{}^0=10^3 M_\odot\,\mathrm{kpc}^{-2})$	All	0-20	$+0.11\pm0.09$	2.40 ± 0.17
$\sigma_{ph}(\mathrm{H\,II})$ $(\sigma_{ph}{}^0=10^{48}\,\mathrm{kpc}^{-2}\,\mathrm{s}^{-1})$	All	0-20	-0.08 ± 0.08	2.06 ± 0.16
Emerson (1974)[2]: $\sigma_N(\mathrm{H\,II})$.....	All			2.23 ± 0.11
Unwin (1980 a, b)[3]: $\sigma_N(\mathrm{H\,II})$.....	All	0-20		1.36 ± 0.09
	All	0-10		1.07 ± 0.10
	All	10-20		1.62 ± 0.07
	Class 1	0-20		1.49 ± 0.10
	Class 2	0-20		1.33 ± 0.12
	Class 3	0-20		1.09 ± 0.09
Berkhuijsen (1977)[4]: $\sigma_N(\mathrm{H\,II})$.....	All	0-21		1.97 ± 0.20
	All	3- 9		2.06 ± 0.06
	All	9-15		2.13 ± 0.37

(1) Surface brightness class defined by Pellet et al. (1978).
(2) HPBW of $1'.5\times2'.2$.
Data of H II regions from Baade and Arp (1964).
(3) HPBW of $0'.8\times1'.2$.
(4) Data of H II regions from Baade and Arp (1964).
Data of H I gas from Emerson (1974), but smoothed to a resolution of $4'.8\times4'.8$.

the galactic plane of M31 into grids with 0.946-kpc widths and count the number of H II regions in each grid cell. In the same grids we calculate mean surface density of the H I gas $\sigma_N(\mathrm{H\,I})$. The number density $\sigma_N(\mathrm{H\,II})$ is plotted against $\sigma_N(\mathrm{H\,I})$ on the logarithmic scale. Then the most probable value and probable error of $\log[\sigma_N(\mathrm{H\,II})]$ are calculated by averaging in given intervals of $\log[\sigma_N(\mathrm{H\,I})]$. The area ratio, the surface mass density, and the surface photon number density are also obtained by the same procedure and plotted against $\sigma_N(\mathrm{H\,I})$.

The relation of $\sigma_N(\mathrm{H\,II})$ to $\sigma_N(\mathrm{H\,I})$ at $R=0$–20 kpc is plotted in figure 10a. From the figure it is clear that a power-law relation is a good fit. Figure 10b shows the same relations separately in the inner ($R=0$–10 kpc) and outer ($R=10$–20 kpc) parts of the galaxy. The slope of the plot for the outer region is much steeper than that for the inner region. Table 4 shows the best-fit values of constants κ and n when the power-law relation is expressed, instead of equation (6), as

$$\sigma_N(\mathrm{H\,II})/\sigma_N{}^0(\mathrm{H\,II})=\kappa[\sigma_N(\mathrm{H\,I})/\sigma_N{}^0(\mathrm{H\,I})]^n\,, \qquad (9)$$

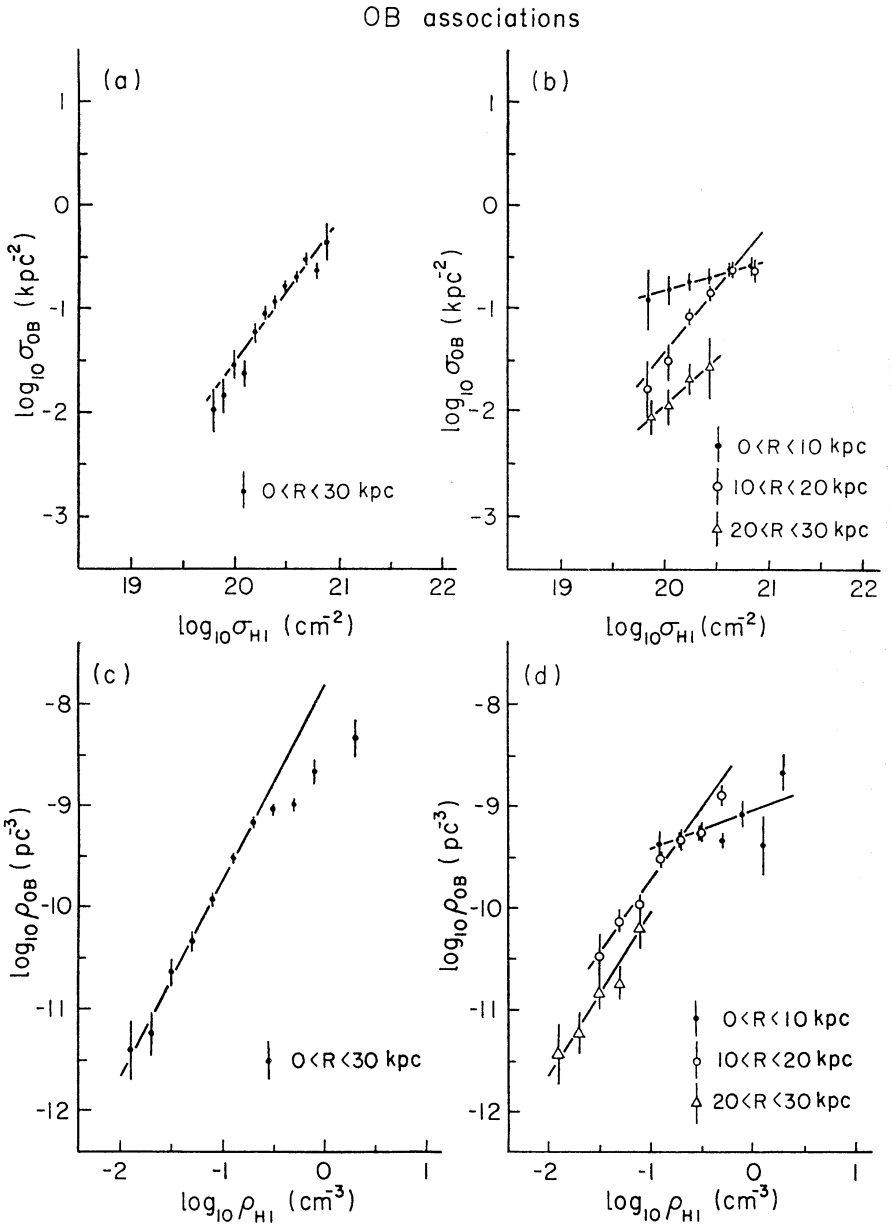

Fig. 11. The relation between σ_N(OB) and σ_N(H I) for (a) the whole galaxy and for (b) $0<R<10$ kpc, $10<R<20$ kpc, and $20<R<30$ kpc, and the relation between ρ_N(OB) and ρ_N(H I) for (c) the whole galaxy and for (d) $0<R<10$ kpc, $10<R<20$ kpc, and $20<R<30$ kpc.

where σ_N^0(H II) and σ_N^0(H I) are constants and set to 1.0 kpc^{-2} and 1.0×10^{20} cm^{-2}, respectively. If we know σ_N(H I) at some place, we can estimate from equation (9) the number density of H II regions there.

The results of other authors are also listed in table 4. Our value of n at $R=0$–20 kpc agrees with the results of Emerson (1974) and Berkhuijsen (1977), but disagrees with those of Unwin (1980a, b). Table 4 also shows the results obtained separately for the three classes of H II regions according to their surface brightness (Pellet et al. 1978). The values of n are not very different from one another. This trend is again contrary to Unwin's (1980b) result.

Table 5. Relation between surface densities of OB associations and H I gas. The same relation is assumed as in table 4.

Physical quantity [σ^0(OB)]	Age	Radius range (kpc)	log κ	n
σ_N(OB) ($\sigma_N{}^0=1.0$ kpc^{-2})	All	0-20	-1.17 ± 0.07	0.81 ± 0.12
	All	0-30	-1.51 ± 0.05	1.37 ± 0.09
	All	0-10	-0.81 ± 0.08	0.29 ± 0.15
	All	10-20	-1.41 ± 0.08	1.23 ± 0.16
	All	20-30	-1.92 ± 0.10	0.89 ± 0.46
	Young	0-30	-2.12 ± 0.10	1.66 ± 0.17
	Intermediate	0-30	-2.47 ± 0.14	1.83 ± 0.23
	Old	0-30	-2.19 ± 0.27	0.50 ± 0.55
	Unclassified	0-30	-1.81 ± 0.08	1.55 ± 0.22
σ_{area}(OB) ($\sigma_{area}{}^0=0.01$).....	All	0-20	-0.17 ± 0.10	1.26 ± 0.19
	All	0-30	-0.48 ± 0.08	1.77 ± 0.17
	Young	0-30	-1.32 ± 0.14	2.31 ± 0.25
	Intermediate	0-30	-0.97 ± 0.16	1.78 ± 0.28
	Old	0-30	-1.35 ± 0.28	1.98 ± 0.62
	Unclassified	0-30	-0.83 ± 0.11	1.59 ± 0.31
Emerson (1974): σ_{area}(OB)	All			0.87 ± 0.07
	Young			1.73 ± 0.08
	Intermediate			0.77 ± 0.26
	Old			—
	Unclassified			0.13 ± 0.17

The presently derived values of n are in agreement with those obtained for other galaxies (e.g. Hamajima and Tosa 1975).

The relations between σ_{area}(H II), σ_M(H II) ($M_\odot$ kpc^{-2}), σ_{ph}(H II) (kpc^{-2} s^{-1}) of H II regions, and σ_N(H I) are also listed in table 4. Larger values of n are obtained for σ_{area}(H II) and σ_M(H II) compared with σ_N(H II), which implies that larger sized and heavier H II regions are situated where σ_N(H I) is larger.

ii) OB associations

Figures 11a and 11b show the relation between σ_N(OB) of OB associations and σ_N(H I) plotted on logarithmic scales (R=0-30 kpc). The best-fit values of κ and n are listed in table 5. The value of n for OB associations is generally smaller than that for H II regions. This trend reflects the radial distribution of OB associations which extends wider than the distribution of H II regions (section 3).

Emerson (1974) examined the relation between σ_N(H I) and estimated surface density of OB stars; the number of stars in an individual OB association was assumed to be proportional to the linear extent of the association along the major axis of M31. He pointed out that the younger the OB associations, the greater is the value of n. Our result for σ_{area}(OB) hows the same trend.

iii) Open clusters

Figure 12a shows the relation of log[σ_N(oc)] of open clusters and log[σ_N(H I)] in R=0-30 kpc. The power-law fitting in figure 12a is not good. This is because of the merging of different power laws at different distance ranges as shown in figure 12b. Table 6 shows the values of κ and n in various distance ranges from

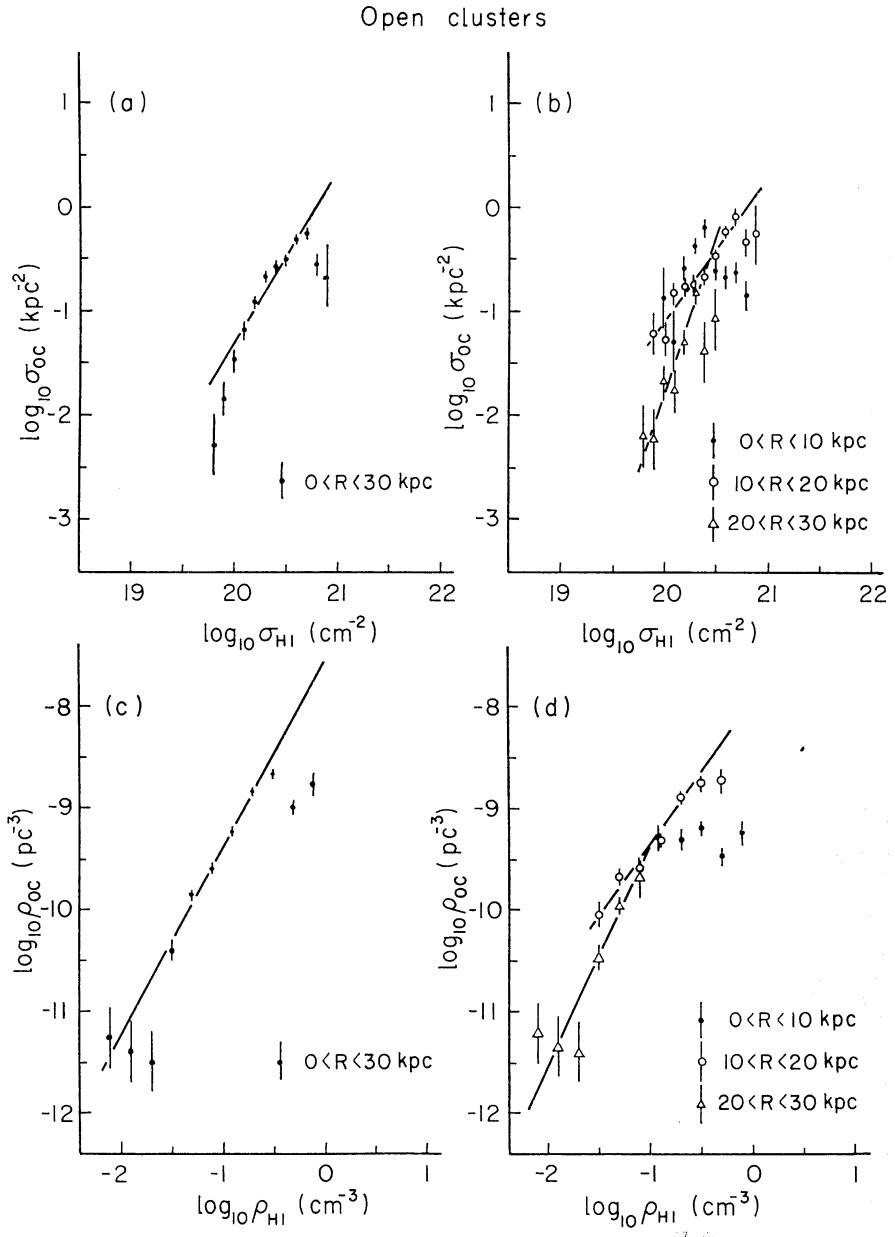

Fig. 12. The same as figure 11 but for open clusters.

the center. The values of n for open clusters lie between n for H II regions and n for OB associations. This corresponds to the degree of concentration on the mean radius $\bar{R}$ (see table 3).

4.2. The Rate of Star Formation Derived from the Volume Densities

In an actual galaxy the thickness of the gas layer where the star formation takes place varies with the radius; this means that the star formation rate derived directly from surface densities might not represent the true value. Here we examine correlations between volume densities of the H I gas and that of optical objects. As mentioned in the beginning of this section, we assume that the volume density of young optical objects, ρ(yo), is a function of volume density of H I, ρ(H I), expressed as a power law:

Table 6. Relation between surface densities of open clusters and H I gas. The same relation is assumed as in table 4.

Physical quantity [σ^0(oc)]	Age	Radius range (kpc)	log κ	n
σ_N(oc) ($\sigma_N{}^0=1.0$ kpc^{-2}).....	All	0-20	-0.92 ± 0.06	0.99 ± 0.12
	All	0-30	-1.29 ± 0.05	1.64 ± 0.10
	All	0-10	—	—
	All	10-20	-1.11 ± 0.06	1.39 ± 0.12
	All	20-30	-1.80 ± 0.10	2.97 ± 0.46

$$\rho(\text{yo})=\kappa\rho(\text{H I})^n . \tag{10}$$

We assume that both the optical objects and H I gas are distributed in the z-direction (perpendicular to the galactic plane) obeying a Gaussian law:

$$\rho(\text{yo})=\rho_0(\text{yo})\exp\{-[z/h(\text{yo})]^2\} \tag{11}$$

and

$$\rho(\text{H I})=\rho_0(\text{H I})\exp\{-[z/h(\text{H I})]^2\} . \tag{12}$$

Here h(yo) and h(H I) are the scale heights of the optical objects and the H I gas in the z direction, respectively. Substituting the above two equations into equation (10), we obtain the following relation (Guibert 1979):

$$h(\text{yo})=h(\text{H I})/n^{1/2} . \tag{13}$$

Remembering that the surface densities are related to the volume densities as

$$\sigma=\int_{-\infty}^{\infty}\rho dz , \tag{14}$$

we obtain

$$\rho(\text{yo})=\sigma(\text{yo})/2h(\text{yo}) \tag{15}$$

and

$$\rho(\text{H I})=\sigma(\text{H I})/2h(\text{H I}) . \tag{16}$$

The H I thickness $2h$(H I) of M31 has been derived by Emerson (1976) as a function of R using a mass model and dispersion velocity of the H I gas. Then we can compute best-fit values of κ and n by an iterative procedure using equation (10), where we can use observed values of σ(yo) and σ(H I) as well as the values of h(H I) from Emerson (1976) to get ρ(yo) and ρ(H I) through equations (13), (15), and (16).

Figures 10c, 10d, 11c, 11d, 12c, and 12d show the logarithmic plots of the volume densities of young optical objects against that of the H I gas. Table 7 lists the best-fit values of κ and n to these plots. The value of n for the outer (R=10–20 kpc for H II regions, R=20–30 kpc for OB associations and open clusters) region derived from the volume densities becomes close to that for the inner (R=0–10 kpc for H II regions, R=10–20 kpc for OB associations and open clusters) region. That is, the difference in the values of n for the inner and outer regions is smaller than that derived from surface densities in subsection 4.1. In particular

Table 7. Relation between volume densities of young optical object and H I gas defined by $\rho(\text{young})/\rho^0(\text{young})=\kappa[\rho_N(\text{H I})/\rho_N{}^0(\text{H I})]^n$, where $\rho_N{}^0(\text{H I})$ is per cubic centimeters.

Object	Physical quantity [ρ^0(yo)]	Radius range (kpc)	log κ	n
H II regions	ρ_N ($\rho_N{}^0=10^{-9}$ pc^{-3})	0-20	1.86±0.07	2.06±0.10
		0-10	0.87±0.07	0.59±0.15
		10-20	1.85±0.08	2.03±0.11
	ρ_{area} ($\rho_{area}{}^0=10^{-3}$ pc^{-1})	0-20	0.32±0.11	2.70±0.15
	ρ_M ($\rho_M{}^0=10^{-3}M_\odot$ pc^{-3})	0-20	0.84±0.13	2.98±0.17
	ρ_{ph} ($\rho_{ph}{}^0=10^{40}$ pc^{-3} s^{-1})	0-20	2.40±0.12	2.66±0.15
OB associations	ρ_N ($\rho_N{}^0=10^{-9}$ pc^{-3})	0-20	0.67±0.09	1.38±0.11
		0-30	1.19±0.11	1.93±0.11
		0-10	−0.05±0.13	0.39±0.22
		10-20	0.66±0.14	1.42±0.15
		20-30	0.58±0.59	1.63±0.39
	ρ_{area} ($\rho_{area}{}^0=10^{-3}$ pc^{-1})	0-30	0.78±0.19	2.29±0.19
Open clusters	ρ_N ($\rho_N{}^0=10^{-9}$ pc^{-3})	0-20	0.94±0.07	1.30±0.08
		0-30	1.43±0.08	1.84±0.08
		0-10	—	—
		10-20	1.04±0.10	1.41±0.10
		20-30	1.84±0.52	2.19±0.38

the power-law relation for open clusters in figure 12c is much better than that in figure 12a. Berkhuijsen (1977) and Guibert (1979) claim that the difference in n for the inner and outer regions vanishes if the volume densities are used. It is interesting to note that the values of n inferred from the three different objects (H II regions, OB associations, open clusters) agree more closely with each other when the volume densities are used than when the surface densities are used.

Comparing figures 10, 11, and 12 we note that the lowest densities of the H I gas necessary for the existence of H II regions, OB associations, and open clusters are about 0.02, 0.012, and 0.008 atoms cm^{-3}, respectively. Also we note that the highest H I density for the existence of H II regions and OB associations is much greater than that for open clusters. These facts indicate that younger objects are more concentrated in denser regions of the H I gas.

In our galaxy it is well known that star formation is significantly correlated not only with atomic hydrogen but also with molecular hydrogen. Actually in our galaxy and M83 a power-law relation holds better for the surface number density of H_2 than for that of H I (Talbot 1980). In M31, however, a power-law fitting between σ_N(H I) alone and σ_N(young objects) seems to be fairly good as seen from figures 10 through 12. Therefore, hydrogen atoms in M31 may be predominantly connected with the star formation. In fact Boulanger et al. (1981) have shown from their CO observations that the fraction of gas in the molecular form is small (7–23%).

5. Summary and Discussion

We have examined relations among various optical data of M31 and the H I gas distribution obtained in Paper I. The optical data contain H II regions, OB associations, open clusters, dark clouds, supernova remnants, and UV photographs. Main results of the present study may be summarized as follows:

(i) Young optical objects (population I objects) and UV emission except dark nebulae are strongly concentrated in the "10-kpc ring" at $R=8$–15 kpc, where about 60 percent of the total H I mass of M31 is involved.

(ii) OB associations and open clusters trace the H I outer arm in SW at $R=18$–26 kpc.

(iii) Most of OB associations are accompanied by H II regions, whereas dark clouds lie generally on the inner edges of strings of H II regions and OB associations.

(iv) Supernova remnants are found only in the spiral arms.

(v) Population I X-ray sources lie on the spiral arms.

(vi) General agreement is seen among the radial distributions of H II regions, OB associations, open clusters, and the H I gas in any sector quadrant of M31 disk.

(vii) However, the weighted mean radius $\bar{R}$ of the radial distributions increases in the order of H II regions ($\bar{R}=10.1$ kpc), OB associations ($\bar{R}=10.7$ kpc), and open clusters ($\bar{R}=11.5$ kpc).

(viii) This fact suggests a galactic-scale shifting of star formation sites: the star formation was most active at $R\simeq 11$–12 kpc about 10^7–10^8 yr ago, while the current star formation is most active at $R\simeq 10$ kpc. This leads to an idea of the galactic-scale propagation of a "star formation ring."

(ix) Concentration of H II regions around $\bar{R}$ is higher than those of OB associations and open clusters. This fact as well as the result (vii) may be related to the difference in the ages of the objects.

(x) Both the surface and volume densities of young optical objects (H II regions, OB associations, open clusters) are well represented by a power-law of the H I density.

(xi) The value of the power-law index n inferred from surface densities is smaller in the inner regions of M31 than in the outer region. When volume densities are used, closer values of n are obtained for the inner and outer regions.

(xii) The values of index n inferred from the three different objects (H II regions, OB associations, open clusters) are different from one another. However, the difference is smaller when the volume densities are used.

From these results some questions may arise about their implications on the evolution, structure, and dynamics of M31 and on the physics of the interstellar space. For example, the positional relationship among dark matter, H II regions, and OB associations on the galactic plane (figure 7) is very complicated and it is difficult to explain it by the galactic shock-wave theory alone. How are they related to one another and how do they affect their formation? What explanation might account for the galactic-scale propagation of a "star formation ring" suggested above? The value of n in equation (1) is one of the most important parameters which determine the evolution of a galaxy. How are the values of n obtained above connected with the spatial distributions of optical objects and the

H I gas? Such questions are problems for further consideration, and will be discussed in a separate paper.

Finally we stress that the present results are valid only for those objects detected in the observation limits. Smaller-sized and/or fainter H II regions, OB associations, open clusters, and dark clouds could possibly be missed as compared with those in our Galaxy and in the Magellanic Clouds. The reader is referred to Pellet et al. (1978), van den Bergh (1964), and Hodge (1979, 1980) for detailed discussions of the completeness of their catalogs and the detection limits in their observations. If the frequency distributions of the diameter and brightness of the optical objects change according to the H I gas densities, the values of index n in equation (1) will change when the observation limits of these objects are improved.

The authors are grateful to Dr. J. M. Deharveng for sending them a new original UV photograph of M31, and to Dr. P. W. Hodge for making the coordinates of open clusters in M31 available prior to publication. They also thank Dr. M. Tosa for his invaluable discussions.

References

Arp, H. 1964, *Astrophys. J.*, **139**, 1045.
Baade, W., and Arp, H. 1964, *Astrophys. J.*, **139**, 1027.
Berkhuijsen, E. M. 1977, *Astron. Astrophys.*, **57**, 9.
Boulanger, F., Stark, A. A., and Combes, F. 1981, *Astron. Astrophys.*, **93**, L1.
Cram, T. R., Roberts, M. S., and Whitehurst, R. N. 1980, *Astron. Astrophys. Suppl.*, **40**, 215.
Deharveng, J. M., Jakobsen, P., Milliard, B., and Laget, M. 1980, *Astron. Astrophys.*, 88, 52.
D'Odorico, S., Dopita, M. A., and Benvenuti, P. 1980, *Astron. Astrophys. Suppl.*, **40**, 67.
Emerson, D. T. 1974, *Monthly Notices Roy. Astron. Soc.*, **169**, 607.
Emerson, D. T. 1976, *Monthly Notices Roy. Astron. Soc.*, **176**, 321.
Guibert, J. 1979, in *Stars and Star Systems*, ed. B. E. Westerlund, (D. Reidel Publishing Company, Dordrecht), p. 85.
Hamajima, K., and Tosa, M. 1975, *Publ. Astron. Soc. Japan*, **27**, 561.
Hodge, P. W. 1979, *Astron. J.*, **84**, 744.
Hodge, P. W. 1980, *Astron. J.*, **85**, 376.
Pellet, A., Astier, N., Viale, A., Courtès, G., Maucherat, A., Monnet, G., and Simien, F. 1978, *Astron. Astrophys. Suppl.*, **31**, 439.
Richter, G. A. 1971, *Astron. Nachr.*, **292**, 275.
Sawa, T., and Sofue, Y. 1981, *Publ. Astron. Soc. Japan*, **33**, 665 (Paper II).
Schmidt, M. 1959, *Astrophys. J.*, **129**, 243.
Simien, F., Athanassoula, E., Pellet, A., Monnet, G., Maucherat, A., and Courtès, G. 1978, *Astron. Astrophys.*, **67**, 73.
Smith, L. F., Biermann, P., and Mezger, P. G. 1978, *Astron. Astrophys.*, **66**, 65.
Sofue, Y., and Kato, T. 1981, *Publ. Astron. Soc. Japan*, **33**, 449 (Paper I).
Spitzer, L., Jr. 1978, in *Physical Processes in the Interstellar Medium* (Wiley, New York), p. 103.
Talbot, R. J., Jr. 1980, *Astrophys. J.*, **235**, 821.
Unwin, S. C. 1980a, *Monthly Notices Roy. Astron. Soc.*, **190**, 551.
Unwin, S. C. 1980b, *Monthly Notices Roy. Astron. Soc.*, **192**, 243.
van den Bergh, S. 1964, *Astrophys. J. Suppl.*, **9**, 65.
Van Speybroeck, L., Epstein, A., Forman, W., Giacconi, R., Jones, C., Liller, W., and Smarr, L. 1979, *Astrophys. J. Letters*, **234**, L45.